

Magnetization dependent tunneling conductance of ferromagnetic barriers

Zhe Wang,^{1,2} Ignacio Gutiérrez-Lezama,^{2,3} Dumitru Dumcenco,² Nicolas Ubrig,^{2,3} Takashi Taniguchi,⁴ Kenji Watanabe,⁵ Enrico Giannini,² Marco Gibertini,^{6,2} and Alberto F. Morpurgo^{2,3}

¹*MOE Key Laboratory for Nonequilibrium Synthesis and Modulation of Condensed Matter, School of Physics, Xi'an Jiaotong University, Xi'an, 710049, China*

²*Department of Quantum Matter Physics, University of Geneva, 24 Quai Ernest Ansermet, CH-1211 Geneva, Switzerland*

³*Group of Applied Physics, University of Geneva, 24 Quai Ernest Ansermet, CH-1211 Geneva, Switzerland*

⁴*International Center for Materials Nanoarchitectonics, National Institute for Materials Science, 1-1 Namiki, Tsukuba, 305-0044, Japan*

⁵*Research Center for Functional Materials, National Institute for Materials Science, 1-1 Namiki, Tsukuba, 305-0044, Japan*

⁶*Dipartimento di Scienze Fisiche, Informatiche e Matematiche, University of Modena and Reggio Emilia, IT-41125 Modena, Italy*

Recent experiments on van der Waals antiferromagnets such as CrI₃, CrCl₃ and MnPS₃ have shown that using atomically thin layers as tunnel barriers and measuring the temperature (T) and magnetic field (H) dependence of the conductance allows their magnetic phase diagram to be mapped. In contrast, barriers made of CrBr₃—the sole van der Waals ferromagnet investigated in this way—were found to exhibit small and featureless magnetoconductance, seemingly carrying little information about magnetism. Here we show that—despite these early results—the conductance of CrBr₃ tunnel barriers does provide detailed information about the magnetic state of atomically thin CrBr₃ crystals for T both above and below the Curie temperature ($T_C = 32$ K). Our analysis establishes that the tunneling conductance depends on H and T exclusively through the magnetization $M(H, T)$, over the entire temperature range investigated (2-50 K). The phenomenon is reproduced in detail by the spin-dependent Fowler-Nordheim model for tunneling, and is a direct manifestation of the spin splitting of the CrBr₃ conduction band. These findings demonstrate that the investigation of magnetism by tunneling conductance measurements is not limited to antiferromagnets, but can also be applied to ferromagnetic materials.

Probing magnetism in atomically thin van der Waals crystals is challenging because most experimental methods commonly employed to study bulk compounds are not sufficiently sensitive to detect any magnetic signal from such a small amount of material¹⁻⁶. Recently, it has been shown that magnetic phase boundaries—and even the complete magnetic phase diagram—of insulating atomically thin magnets can be detected by using them as tunnel barriers, and measuring their temperature-dependent magnetoconductance⁷⁻¹⁵. The sensitivity of the tunneling magnetoconductance to magnetism originates from the dependence of the tunneling probability on the magnetic state¹⁶. As H and T are varied across a magnetic transition, the alignment of the spins in the barrier changes sharply, and so does the tunneling prob-

ability of electrons with different spin orientations. The net result is an equally sharp change in the measured conductance that can be traced to identify the phase boundary.

These conclusions have been drawn from experiments on different antiferromagnetic insulators (CrI₃⁷⁻⁹, CrCl₃¹⁰⁻¹³ and MnPS₃¹⁵), and it is not at all clear that the technique can be equally effective to probe ferromagnetic insulators, since in that case no magnetic phase boundaries are present below the Curie temperature. Indeed, tunneling conductance measurements on ferromagnetic CrBr₃ barriers have shown only an extremely small and featureless low-temperature tunneling magnetoconductance^{13,14,17}, and no pronounced effect was observed, which could be related to magnetism without microscopic modeling. In contrast to this early results, here we show directly from experimental data that the temperature and magnetic field dependence of the tunneling conductance of ferromagnetic CrBr₃ barriers is entirely determined by the magnetization of the material, and can be used to extract detailed, quantitative information both above and below the Curie temperature.

CrBr₃ is a van der Waals layered material that—irrespective of thickness (i.e., from bulk down to monolayer)—exhibits a transition to a ferromagnetic state with an easy axis perpendicular to the layers¹⁸⁻²⁶ (see Fig. 1a, Supplementary Note 1 and Supplementary Fig. 1). Bulk magnetization measurements in Fig. 1b show that the Curie temperature of our crystals is $T_C \simeq 32$ K, with a saturation magnetization corresponding to a magnetic moment of $3\mu_B$ per chromium atom, in line with previous reports¹⁸⁻²¹. Single crystals are exfoliated into thin layers and used to nano-fabricate hBN-encapsulated graphite/CrBr₃/graphite tunnel junctions inside a glove box (see inset of Fig. 1c for a scheme, Supplementary Fig. 2 for an optical image of the device, and Methods for detailed information about device assembly). Fig. 1c presents the current-voltage (I - V) characteristics for two representative devices with different thickness d (corresponding to $N = 7$ and 8 layers), showing typical tunneling transport at low temperatures and the scaling behavior predicted by the Fowler-Nordheim

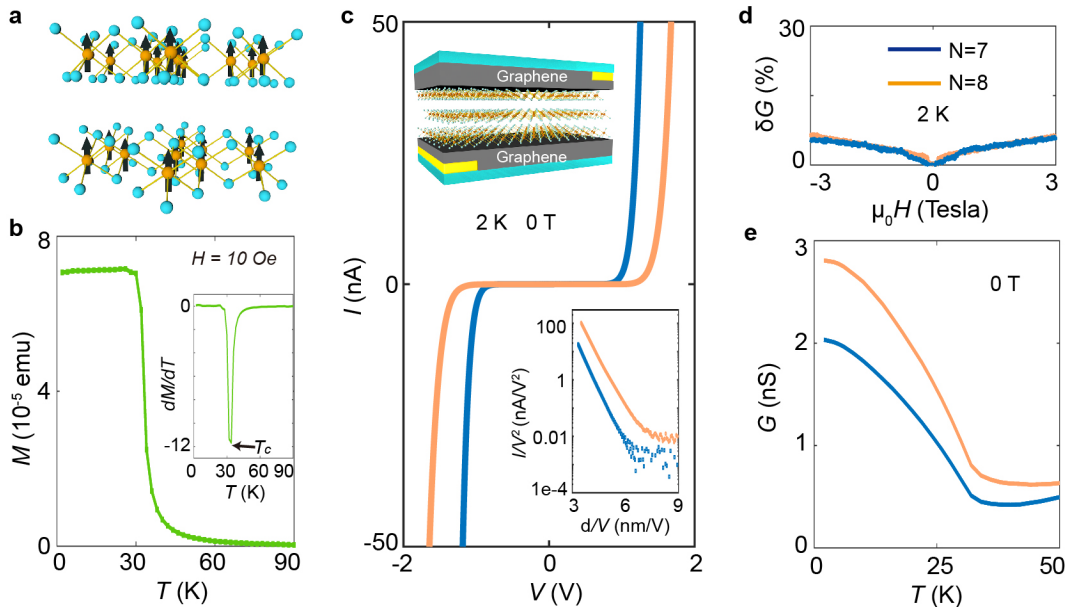


Fig. 1. Tunneling conductance of CrBr₃ multilayers. **a:** Schematics of the crystal structure of CrBr₃: the orange balls represent the Cr atoms with the associated spins pointing perpendicularly to the layers; the light blue balls represent the Br atoms. **b:** Temperature dependence of the magnetization measured on bulk CrBr₃ crystals with a magnetic field of 1 mT applied perpendicular to the layers. The inset shows the plot of dM/dT , with a sharp minimum close to 32 K, corresponding to the Curie temperature of CrBr₃. **c:** Tunneling current as a function of applied voltage measured on a 7 (blue curve) and 8 (orange curve) layer CrBr₃ device at $T = 2$ K (curves of the same color in panels **d** and **e** represent data measured on the same devices). The up left insert is a cartoon representation of our hBN-encapsulated graphene/CrBr₃/graphene tunnel junction devices. The down right insert shows that –for sufficiently large applied bias V – $\log(I/V^2)$ is linearly proportional to d/V (d is the thickness of CrBr₃), as expected in the Fowler-Nordheim tunneling regime. **d:** Magnetoconductance $\delta G(H, T) \equiv [G(H, T) - G(0, T)]/G(0, T)$ measured at $T = 2$ K, on the 7 and 8 layer devices. **e:** Temperature dependence of the zero-field tunneling conductance of the 7 and 8 layer devices, exhibiting an increase of approximately 300 %, as T is lowered from T_C to 2 K. Data in panels **d** and **e** have been acquired with an applied bias voltage $V = 1$ V and $V = 1.4$ V for the 7 and 8 layer devices, respectively.

tunneling formula (i.e., $\log(I/V^2) \propto d/V$)^{27,28}. As shown in Fig. 1d, application of an external magnetic field up to 3 T at $T = 2$ K causes only minor (<6%) and featureless variations in the conductance $G = I/V$. This is consistent with previous reports^{13,14} and expected for a ferromagnetic semiconductor, in which –at low temperature– the spins are spontaneously fully polarized already in the absence of an applied magnetic field.

Despite the negligible low-temperature magnetoconductance, Fig. 1e shows that the conductance measured at zero applied magnetic field $G(H = 0, T)$ increases by a factor of three as T is lowered from the Curie temperature $T_C = 32$ K down to 2 K. As the conductance is virtually temperature independent above T_C (for $32 < T < 50$ K), we infer directly from the experimental data that the conductance increase is due to CrBr₃ entering the ferromagnetic state. This observation implies that magnetism does influence the electrical conductance of the tunnel barriers and that the effect is sizable: a threefold increase in conductance is comparable to the magnetoresistance of most common magnetic tunnel junctions (i.e., tunneling spin valve devices²⁹) and of CrCl₃ antiferro-

magnetic tunnel barriers^{10–14}.

This observation motivates us to look more in detail at the temperature-dependent magnetoconductance of CrBr₃ barriers, $\delta G(H, T) \equiv [G(H, T) - G(0, T)]/G(0, T)$. The full dependence of $\delta G(H, T)$ on T and H is shown in Fig. 2a for both the 7- and 8-layer CrBr₃ devices, with the two of them exhibiting identical behavior. In both devices, $\delta G(H, T)$ is positive and peaks at $T = T_C$ irrespective of the applied magnetic field H . The positive magnetoconductance can be understood, since at high T the application of a magnetic field does lead to a better alignment of the spins in CrBr₃. Similarly to what happens in CrI₃ and CrCl₃ tunnel barriers, a better spin alignment enhances the tunneling probability, causing the conductance to increase. We note that when T approaches T_C from above –coming from the paramagnetic state of CrBr₃– the magnetic field required to increase the conductance systematically decreases, indicating that the spin susceptibility χ is enhanced. This trend is reminiscent of the behavior expected from the critical fluctuations in the neighborhood of the ferromagnetic transition³⁰.

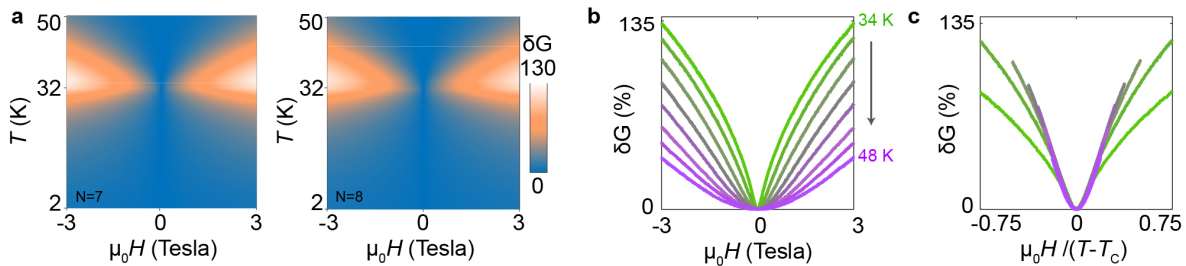


Fig. 2. Temperature evolution of the tunneling magnetoconductance. **a:** Color plot of tunneling magnetoconductance for the 7 (left) and 8 layer (right) device as a function of applied magnetic field $\mu_0 H$ and temperature T . At fixed applied field, the magnetoconductance is maximum close to $T_c = 32$ K. **b:** Magnetoconductance of 7 layer device for $T > T_c$, as T is varied from 34 to 48 K, in 2 K steps. **c:** when plotted as a function of $\mu_0 H / (T - T_c)$, the magnetoconductance curves shown in panel **b** collapse on top of each other at small field, indicating that in the linear regime the magnetoconductance $\delta G(H, T)$ depends on H and T only through the magnetization $M(H, T)$. In panels **b** and **c**, curves of the same color correspond to measurements done at the same temperature.

The idea that the magnetoconductance for $T > T_C$ probes the fluctuations of the spins in the critical regime of the paramagnetic state can be tested quantitatively if we recall that in a mean-field description of this regime, the linear spin polarizability $\chi \propto 1/(T - T_C)$ as T approaches T_C ³⁰. We can then check whether the conductance depends on the magnetic field induced spin polarization, or equivalently on the magnetization (whose mean-field expression is given by the Curie-Weiss law, $M \propto \mu_0 H / (T - T_C)$), by simply plotting $\delta G(H, T)$ as a function of $\mu_0 H / (T - T_C)$ for any $T > T_C$ (see Fig. 2b). For sufficiently small $\mu_0 H / (T - T_C)$ all curves indeed collapse on top of each other (Fig. 2c), irrespective of the temperature at which they are measured, confirming that in the linear regime the field-induced increase of the conductance is determined by the net spin polarization (i.e., by the field-induced magnetization).

The relation between magnetoconductance and magnetization can be tested beyond the linear regime, by using the magnetization $M(H, T)$ measured on bulk crystals (Fig. 3b) to re-plot the magnetoconductance of our tunnel barriers $\delta G(H, T)$ (Fig. 3a) as a function of M . The result is shown in Fig. 3c, with curves of different colors representing magnetoconductance measurements done at different temperatures. When plotted as a function of M all curves collapse on top of each other throughout the entire range of H and $T > T_C$ investigated. We can therefore conclude directly from the data that the magnetoconductance δG depends on H and T only through the magnetization $M(H, T)$ even well outside the linear regime. That is: for $T > T_C$, $\delta G(H, T) = \delta G(M(H, T))$.

To extend our analysis from the paramagnetic state to $T < T_C$, when the CrBr_3 barriers are ferromagnetic, we look at the temperature dependence of the conductance measured at zero applied field. To this end, we consider the quantity $\Delta G(H, T) \equiv [G(0, T) - G(0, T_C)] / G(0, T_C)$, i.e., the relative increase in conductance observed as T is lowered below the Curie temperature. If the conductance is a function of magnetization, this function should

be the same underlying the behavior of $\delta G(H, T)$ for $T > T_C$, because the temperature dependence of $G(0, T)$ originates exclusively from the temperature dependence of the spontaneous magnetization $M(H = 0, T)$, which in the ferromagnetic state increases from zero at $T = T_C$, to its saturation value for $T \ll T_C$. Consistently with this idea, the data in Fig. 1e shows an increase in conductance upon lowering T . However, to establish whether the functional dependence of the magnetoconductance on magnetization below T_C is the same as the one found for $T > T_C$ a more quantitative analysis is needed.

For such an analysis we cannot rely on the magnetization measured on bulk crystals, because in the ferromagnetic state the magnetization of bulk samples at $H = 0$ is entirely determined by the formation of magnetic domains^{30,31}, whereas exfoliated atomically thin crystals of the size used in our devices have been found to behave as single domains^{22,25,26}. Indeed, magnetization measurements on CrBr_3 bulk crystals for $T < T_C$ exhibit virtually no remnant magnetization nor any hysteresis upon cycling the applied magnetic field (see Supplementary Fig. 1), whereas Hall magnetometry of atomically thin, exfoliated CrBr_3 crystals exhibit finite remnant magnetization and a clear hysteresis²². That is why in what follows we use the temperature-dependent, zero-field magnetization obtained in Hall magnetometry experiments that –as discussed in Ref. 22– is very well reproduced by the temperature dependence calculated using the XXZ model with anisotropic exchange interaction, shown in Fig. 3e.

We use the spontaneous magnetization curve shown in Fig. 3e to re-plot the quantity $\Delta G(H, T)$ shown in Fig. 3d, as a function of M . The result is represented by the open circles in Fig. 3c. The data fall on top of the $\delta G(M)$ curve found in our analysis of transport in the paramagnetic state of CrBr_3 , for $T > T_C$. The excellent agreement demonstrates that the conductance of CrBr_3 tunnel barriers depends on temperature and magnetic field only through its magnetization over the full experimental range investigated, and that the dependence

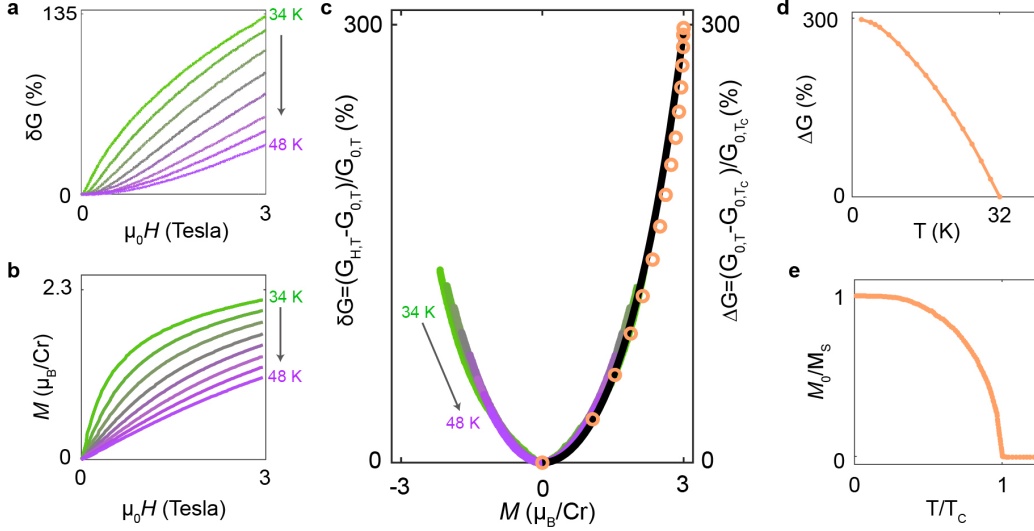


Fig. 3. Magnetization dependence of tunneling magnetoconductance. **a:** Tunneling magnetoconductance measured for $T > T_c$, as T is varied from 34 K to 48 K in 2 K steps (curves of the same color in panels **b** and **c** represent measurements taken at the same temperature). **b:** Magnetic field dependence of the magnetization measured on bulk CrBr₃ crystals. **c:** Magnetization dependence of tunneling magneto-conductance. Colored lines represent the magnetoconductance measured at different $T > T_c$, plotted as a function of the bulk magnetization measured at the same temperature. The orange open circles represent the relative change in conductance due to the increase in the spontaneous magnetization of CrBr₃, measured for different $T < T_c$, obtained from the data shown in panels **d** and **e**. All data collapse on top of each other, indicating that the conductance is a function of the magnetization, i.e. it depends on H and T exclusively through $M(H, T)$, throughout the entire T range investigated (i.e., from well below to well above T_c). The black line is a fit based on the expression obtained from the spin-dependent Fowler-Nordheim tunneling model, under the assumption that the splitting between the spin up and down bands is proportional to the magnetization (see main text for details). **d:** Temperature dependence of the relative conductance increase as T is lowered below T_c , in the ferromagnetic state of CrBr₃. **e:** Spontaneous magnetization of CrBr₃ calculated by XXZ model with anisotropic exchange interactions that –as shown in Ref. 22– accurately reproduces the measured magnetization of atomically thin CrBr₃ crystals .

is described by the same function from well above T_c to the lowest temperature reached in our measurements (2 K). This conclusion is extremely robust, because it is drawn directly from the analysis of the experimental data, without any theoretical assumption (the 8-layer device exhibits an identical behavior, as discussed in Supplementary Note 3 and shown in Supplementary Fig. 5).

These experimental results have a straightforward interpretation within the context of Fowler-Nordheim (FN) tunneling transport commonly used to interpret the conductance of van der Waals magnetic barriers. In FN tunnelling, the applied bias tilts the conduction band across the CrBr₃ layer, effectively reducing the thickness of the tunnel barrier, so that eventually the tunneling probability for electrons becomes sizable and a finite current is observed^{27,28}. The $I - V$ characteristics in the FN tunneling regime satisfy the relation:

$$I \propto \frac{V^2}{\phi_B} e^{-\frac{8\pi d\sqrt{2m^*}\phi_B^{3/2}}{3\hbar eV}}, \quad (1)$$

where m^* is the effective mass describing the motion of electrons in CrBr₃ in the direction perpendicular to the

planes, ϕ_B is the barrier height determined by the distance between the Fermi level in the contacts and the conduction band edge in CrBr₃, \hbar is Planck's constant and e the (modulus of the) electron charge. For a ferromagnet, an analogous relation is expected to hold separately for electrons with spin up and spin down, which experience different barrier heights ϕ_\uparrow and ϕ_\downarrow , due to the spin-splitting of the conduction band present for $T < T_c$ (see Fig. 4a). The total conductance is then given by the sum of the contributions given by electrons with spin up and spin down :

$$G = G^\uparrow + G^\downarrow = A \frac{V}{\phi_\uparrow} e^{-\frac{8\pi d\sqrt{2m^*}\phi_\uparrow^{3/2}}{3\hbar eV}} + A \frac{V}{\phi_\downarrow} e^{-\frac{8\pi d\sqrt{2m^*}\phi_\downarrow^{3/2}}{3\hbar eV}}, \quad (2)$$

where A is a constant determined by the barrier dimensions.

We use this expression to analyze the experimental data by assuming that the spin splitting of the conduction band in the ferromagnetic state is linearly proportional to the magnetization, resulting in barrier heights for spin up and down given by $\phi_{\uparrow,\downarrow} = \phi_{B0} \pm \gamma M$. We calculate the magnetoconductance $[G(M) - G(M = 0)]/G(M = 0)$

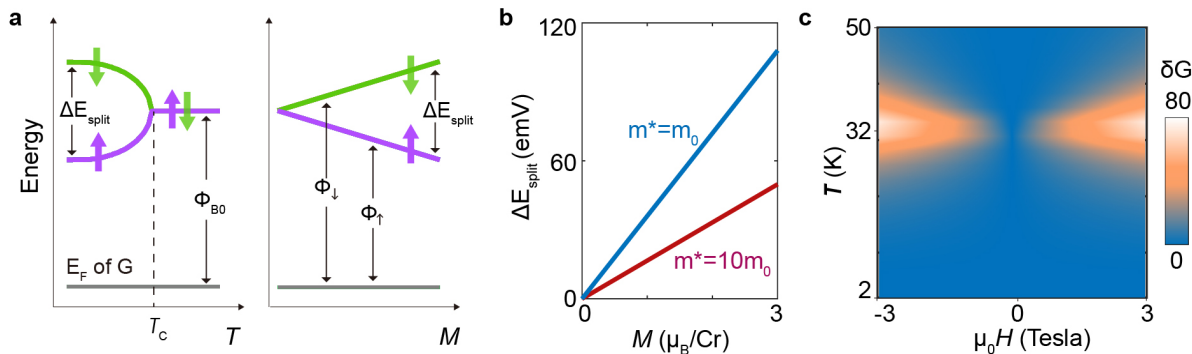


Fig. 4. Relation between spin splitting energy and magnetization. **a:** Schematic diagram of the relevant energies involved in tunneling process. The spin-up and spin-down CrBr₃ conduction bands become non-degenerate when the magnetization M is finite, causing a different height of the tunneling barrier for electrons whose spin points in opposite directions (the barrier height is given by the distance between the corresponding band edge and the Fermi level E_F in the graphene electrodes, indicated by the bottom horizontal line). A finite M can be induced by the appearance of the spontaneous magnetization as T is lowered below T_C , or by the application of an external magnetic field for $T > T_C$. **b:** Magnetization dependence of the splitting energy, as determined from fitting of the data in Fig. 3c using the spin-dependent Fowler-Nordheim tunneling model to model the conductance. The blue and purple lines correspond to the results obtained assuming the effective mass in the direction perpendicular to the layers of CrBr₃ to be m_0 or $10m_0$, respectively. **c:** Color map of magnetoconductance calculated using Eq. (2) in the main text, using the Weiss model to determine the dependence $M(H, T)$ of the magnetization on magnetic field and temperature.

using the value of $\sqrt{2m^*}\phi_{B0}$ extracted from the measured $I - V$ curves, and treating γ as the sole fitting parameter. The result of this procedure –represented by the black curve in Fig. 3c– reproduces the experimental data perfectly. Interestingly, a conceptually similar approach has been followed in earlier beautiful work on the tunneling conductance of EuO barriers in the ferromagnetic state³². That work, however, focused exclusively on the case of $T < T_C$ and zero applied magnetic field, by analyzing the temperature dependence of the conductance in terms of the measured temperature dependence of the magnetization. Our results show that the approach has a much broader validity: it can be applied both below and above T_C , it remains valid in the presence of a magnetic field, and –as CrBr₃ and EuO are very different materials– it describes very different classes of ferromagnetic insulators. If used in conjunction with a model predicting the magnetic field and temperature dependence of the magnetization, this approach allows the full magnetoconductance to be calculated. This is illustrated by the color plot in Fig. 4d that –despite having been obtained with the simplest possible Weiss model of Ising ferromagnetism– reproduces all the qualitative features observed in the experiments (compare Fig. 4d with Fig. 2a), and even exhibits a nearly quantitative agreement. Alternatively, it is also possible to extract the temperature and magnetic field dependence of the magnetization from the measured magnetoconductance, as discussed in Supplementary Note 2 and shown in Supplementary Fig. 4.

The excellent agreement between the calculated and the measured magnetoconductance (see Fig. 3c) suggests the possibility to extract the spin splitting energy quan-

titatively, from the value of the fitting parameter γ . This is however not straightforward, because Eq. (2) depends on the product $\sqrt{m^*}(\phi_0)^{3/2}$, and the effective mass m^* is not known. Fig. 4b shows the spin splitting energy as a function of magnetization obtained by taking the value of γ used to fit the $\delta G = \delta G(M)$ curves in Fig. 3c, and assuming the effective mass m^* to be either the free electron mass m_0 or $10m_0$, a very large value chosen to mimic the flatness of the CrBr₃ bands in the direction perpendicular to the layers^{33,34}. We find that at saturation the energy splitting separating the spin-up and the spin-down bands is approximately 110 meV if $m^* = m_0$ and 50 meV if $m^* = 10m_0$, indicating that for realistic values of the effective mass the spin-splitting energy is between 50 and 110 meV. We emphasize, however, that care is certainly needed in interpreting the meaning of this quantity microscopically, because –as applied to CrBr₃ barriers– the Fowler-Nordheim model is a phenomenological approach that does not take into account the complexity of the microscopic electronic structure of the material. In particular, it does not take into account that the conduction band consists of two distinct, nearly degenerate electronic bands originating from the e_{1g} and t_{2g} orbitals of the Cr atoms.

Irrespective of these details, the key result presented here is that the measured tunneling magnetoconductance of CrBr₃ is entirely determined by its magnetization, which is why magnetoconductance measurements can be used to investigate the magnetic properties of the material. We envision, for instance, that magnetoconductance measurements will allow detailed investigations of the critical behavior of the magnetic susceptibility in the paramagnetic state for T very close to T_C and provide a

new, experimentally simple way to determine critical exponents. This is possible because the required data analysis only relies on the fact that at small M the magnetoconductance is a quadratic function of the magnetization (see Supplementary Note 2 and Supplementary Fig. 3). Another interesting possibility is to analyze magnetoconductance measurements over a broad range of temperatures and magnetic fields, to discriminate between microscopic theoretical models that predict a different

functional dependence for $M(H, T)$ (see Supplementary Note 2 and Supplementary Fig. 4). These are just two examples that illustrate the most important aspect of our results, namely that measurements of the tunneling conductance are not limited to the investigation of antiferromagnetic barriers, but can also provide detailed information about the magnetic properties of ferromagnetic insulators.

-
- ¹ Burch, K. S., Mandrus, D. & Park, J.-G. Magnetism in two-dimensional van der Waals materials. *Nature* **563**, 47–52 (2018).
- ² Gong, C. & Zhang, X. Two-dimensional magnetic crystals and emergent heterostructure devices. *Science* **363** (2019).
- ³ Gibertini, M., Koperski, M., Morpurgo, A. & Novoselov, K. Magnetic 2D materials and heterostructures. *Nature Nanotechnology* **14**, 408–419 (2019).
- ⁴ Mak, K. F., Shan, J. & Ralph, D. C. Probing and controlling magnetic states in 2D layered magnetic materials. *Nature Reviews Physics* **1**, 646–661 (2019).
- ⁵ Avsar, A. *et al.* Colloquium: Spintronics in graphene and other two-dimensional materials. *Reviews of Modern Physics* **92**, 021003 (2020).
- ⁶ Huang, B. *et al.* Emergent phenomena and proximity effects in two-dimensional magnets and heterostructures. *Nature Materials* **19**, 1276–1289 (2020).
- ⁷ Song, T. *et al.* Giant tunneling magnetoresistance in spin-filter van der Waals heterostructures. *Science* **360**, 1214–1218 (2018).
- ⁸ Klein, D. R. *et al.* Probing magnetism in 2D van der Waals crystalline insulators via electron tunneling. *Science* **360**, 1218–1222 (2018).
- ⁹ Wang, Z. *et al.* Very large tunneling magnetoresistance in layered magnetic semiconductor CrI_3 . *Nature Communications* **9**, 1–8 (2018).
- ¹⁰ Wang, Z. *et al.* Determining the phase diagram of atomically thin layered antiferromagnet CrCl_3 . *Nature Nanotechnology* **14**, 1116–1122 (2019).
- ¹¹ Cai, X. *et al.* Atomically thin CrCl_3 : an in-plane layered antiferromagnetic insulator. *Nano Letters* **19**, 3993–3998 (2019).
- ¹² Klein, D. R. *et al.* Enhancement of interlayer exchange in an ultrathin two-dimensional magnet. *Nature Physics* **15**, 1255–1260 (2019).
- ¹³ Kim, H. H. *et al.* Evolution of interlayer and intralayer magnetism in three atomically thin chromium trihalides. *Proceedings of the National Academy of Sciences* **116**, 11131–11136 (2019).
- ¹⁴ Kim, H. H. *et al.* Tailored tunnel magnetoresistance response in three ultrathin chromium trihalides. *Nano Letters* **19**, 5739–5745 (2019).
- ¹⁵ Long, G. *et al.* Persistence of magnetism in atomically thin MnPS_3 crystals. *Nano Lett.* **20**, 2452–2459 (2020).
- ¹⁶ Moodera, J. S., Santos, T. S. & Nagahama, T. The phenomena of spin-filter tunnelling. *Journal of Physics: Condensed Matter* **19**, 165202 (2007).
- ¹⁷ Ghazaryan, D. *et al.* Magnon-assisted tunnelling in van der Waals heterostructures based on CrBr_3 . *Nature Electronics* **1**, 344–349 (2018).
- ¹⁸ Tsubokawa, I. On the magnetic properties of a CrBr_3 single crystal. *Journal of the Physical Society of Japan* **15**, 1664–1668 (1960).
- ¹⁹ Jennings, L. & Hansen, W. Heat capacity of CrBr_3 from 14 to 360°K . *Physical Review* **139**, A1694 (1965).
- ²⁰ Ho, J. T. & Litster, J. D. Divergences of the magnetic properties of CrBr_3 near the critical point. *Journal of Applied Physics* **40**, 1270–1271 (1969).
- ²¹ Samuelsen, E., Silbergliitt, R., Shirane, G. & Remeika, J. Spin waves in ferromagnetic CrBr_3 studied by inelastic neutron scattering. *Physical Review B* **3**, 157 (1971).
- ²² Kim, M. *et al.* Micromagnetometry of two-dimensional ferromagnets. *Nature Electronics* **2**, 457–463 (2019).
- ²³ Chen, W. *et al.* Direct observation of van der Waals stacking-dependent interlayer magnetism. *Science* **366**, 983–987 (2019).
- ²⁴ Zhang, Z. *et al.* Direct photoluminescence probing of ferromagnetism in monolayer two-dimensional CrBr_3 . *Nano Letters* **19**, 3138–3142 (2019).
- ²⁵ Jin, C. *et al.* Imaging and control of critical fluctuations in two-dimensional magnets. *Nature Materials* **19**, 1290–1294 (2020).
- ²⁶ Sun, Q.-C. *et al.* Magnetic domains and domain wall pinning in atomically thin CrBr_3 revealed by nanoscale imaging. *Nature Communications* **12**, 1989 (2021).
- ²⁷ Fowler, R. H. & Nordheim, L. Electron emission in intense electric fields. *Proceedings of the Royal Society of London. Series A, Containing Papers of a Mathematical and Physical Character* **119**, 173–181 (1928).
- ²⁸ Lenzlinger, M. & Snow, E. Fowler-Nordheim tunneling into thermally grown SiO_2 . *Journal of Applied Physics* **40**, 278–283 (1969).
- ²⁹ Žutić, I., Fabian, J. & Sarma, S. D. Spintronics: Fundamentals and applications. *Reviews of Modern Physics* **76**, 323 (2004).
- ³⁰ Blundell, S. *Magnetism in condensed matter* (Oxford University Press, 2003).
- ³¹ Kuhlow, B. & Lambeck, M. Magnetic domain structures in CrBr_3 . *Physica B+ C* **80**, 365–373 (1975).
- ³² Santos, T. *et al.* Determining exchange splitting in a magnetic semiconductor by spin-filter tunneling. *Physical Review Letters* **101**, 147201 (2008).
- ³³ Wang, H., Eyert, V. & Schwingenschlögl, U. Electronic structure and magnetic ordering of the semiconducting chromium trihalides CrCl_3 , CrBr_3 , and CrI_3 . *Journal of Physics: Condensed Matter* **23**, 116003 (2011).
- ³⁴ Soriano, D., Katsnelson, M. I. & Fernández-Rossier, J. Magnetic two-dimensional chromium trihalides: A theo-

retical perspective. *Nano Letters* **20**, 6225–6234 (2020).

Methods

Bulk crystal growth and characterizations

Crystals of CrBr_3 were grown by the Chemical Vapour Transport method as reported earlier. Pure Chromium (99.95% CERAC) and TeBr_4 (99.9% Alfa Aesar) were mixed with a molar ratio 1 : 0.75 to a total mass of 0.5 g, and put in quartz tube with an internal diameter of 10 mm and a length of 13 cm. The preparation of the quartz reactor was done inside a glove box under pure Ar atmosphere. The tube was evacuated down to 10^{-4} mbar and sealed under vacuum, then put in a horizontal tubular furnace in a temperature gradient of about $10^\circ\text{C}/\text{cm}$, with the hot end at 700°C and the cold end at 580°C . After 7 days at this temperature, the furnace was switched off, and the tube cooled to room temperature. CrBr_3 was found to crystallise at the cold end of the tube. Shiny, thin platelet-like, dark green-blackish single crystals of typical lateral size of 2-5 mm were extracted. Bulk crystals of 2.1 mg were used for the magnetic characterization in a MPMS3 SQUID magnetometer (Quantum Design). The magnetic moment of the crystals was measured with magnetic field parallel to the crystallographic *c*-axis.

Tunneling junction fabrication and transport measurements

CrBr_3 multilayers were mechanically exfoliated from the crystals discussed in the section of crystal growth. Tunnel junctions of multilayer graphene/ CrBr_3 /multilayer graphene were assembled using a pick-and-lift technique with stamps of PDMS/PC. To avoid degradation of thin CrBr_3 multilayers, the exfoliation of CrBr_3 and the heterostructure stacking process were done in a glove box filled with Nitrogen gas, and the whole tunneling junction was encapsulated with hBN before being taken out. Conventional electron beam lithography, reactive-ion etching,

electron-beam evaporation (10 nm/50 nm Cr/Ar) and lift-off process were used to make edge contacts to the multilayer graphene. The thickness of the layers was determined by atomic force microscope measurements performed outside the glove box, on the encapsulated devices. Transport measurements were performed in a cryostat from Oxford Instruments, using home-made low-noise electronics.

Data availability

All relevant data are available from the corresponding authors upon reasonable and well-motivated request.

Acknowledgements

We sincerely acknowledge Alexandre Ferreira for technical support. Z.W. acknowledges the National Natural Science Foundation of China (Grants no. 11904276). A.F.M. gratefully acknowledges financial support from the Swiss National Science Foundation (Division II) and from the EU Graphene Flagship project. M.G. acknowledges support from the Italian Ministry for University and Research through the Levi-Montalcini program. K.W. and T.T. acknowledge support from the Elemental Strategy Initiative conducted by the MEXT, Japan, Grant Number JPMXP0112101001 and JSPS KAKENHI Grant Number JP20H00354.

Author contributions

Z.W. and A.F.M. conceived the work. D.D. and E.G. grew CrBr_3 crystals and performed bulk characterization. T.T. and K.W. provided high-quality boron nitride crystals. Z.W. fabricated samples and performed transport measurements with help of I.G. and N.U.. Z.W., I.G., N.U., M.G. and A.F.M. analyzed and interpreted the magnetoconductance data. All authors contributed to writing the manuscript.

Competing interests

The authors declare no competing interests.